Published in IET Signal Processing
Received on 10th April 2009
Revised on 30th August 2009
doi: 10.1049/iet-spr.2009.0104

Special Issue on Time-Frequency Approach to Radar Detection, Imaging, and Classification

ISSN 1751-9675

Accurate and efficient implementation of the time–frequency matched filter

J.M. O' Toole[1] *M. Mesbah*[1] *B. Boashash*[2,*]

[1]*The University of Queensland, Perinatal Research Centre and UQ Centre for Clinical Research, Royal Brisbane & Women's Hospital, Herston, QLD 4029, Australia*
[2]*College of Engineering, Qatar University, P.O. Box 2713, Doha, Qatar*
[*]*Also with the University of Queensland*
E-mail: j.otoole@ieee.org

Abstract: The discrete time–frequency matched filter should replicate the continuous time–frequency matched filter, but the methods differ. To avoid aliasing, the discrete method transforms the real-valued signal to the complex-valued analytic signal. The theory for the time–frequency matched filter does not consider the discrete case using the analytic signal. The authors find that the performance of the matched filter degrades when using the analytic, rather than real-valued, signal. This performance degradation is dependent on the signal-to-noise ratio and the signal type. In addition, the authors present a simple algorithm to efficiently compute the time–frequency matched filter. The algorithm with the real-valued signal, comparative to using the analytic signal, requires one-quarter of the computational load. Hence the real-valued signal – and not the analytic signal – enables an accurate and efficient implementation of the time–frequency matched filter.

1 Introduction

The time–frequency matched filter is used to detect signals in a noisy environment. Important applications for this detection method include radar and sonar systems [1–3]. To compute the time–frequency matched filter, we require a discrete version of this matched filter. The discrete time–frequency matched filter uses the analytic associate of the real-valued signal to avoid aliasing [1, 4, 5]. However, the effect on the performance of using this analytic signal has yet to be determined. Also, the two-dimensional matched filter requires a large computational load to compute. This article addresses the two important issues of accurate and efficient computation of the time–frequency matched filter.

The time-domain matched filter, often refered to as the ambiguity function [6], is used to detect a known signal embedded in noise [7]. The time–frequency matched filter extends the time-domain filter to incorporate both time–frequency smoothing and filtering. This matched filter can outperform the time-domain method when we relax some of the strict conditions on the time-domain matched filter [8]. Thus the time–frequency matched filter is applicable to a larger set of detection scenarios. Examples include detecting a radar signal that is transmitted through a randomly time-varying channel, or detecting a passive sonar signal that is not exactly known but inferred from noisy measurements. For these detection scenarios, the time–frequency matched filter will outperform the time-domain matched filter [8, 9].

The time–frequency matched filter correlates, in time and frequency, a time–frequency distribution (TFD) of the received signal with a TFD of the known signal. A TFD is a representation of the signal's energy in the joint time–frequency domain. The discrete matched filter correlates discrete TFDs (DTFDs). To avoid aliasing, the DTFDs use the complex-valued analytic associate of the real-valued signal [10–13]. What effect does this mapping from real-valued to analytic signal have on the performance of the discrete matched filter?

We show that using the analytic signal, rather than the real-valued signal, degrades the performance of the discrete

matched filter. We infer this statement from experimental results using a set of example signals. The results show that the performance degradation was greater at smaller signal-to-noise ratios (SNRs) compared with the performance degradation at higher SNRs. We should therefore correlate two aliased, and not alias-free, DTFDs to form the matched filter.

We also propose a computationally efficient algorithm to compute the time–frequency matched filter. The algorithm, for N-point signals, requires a computational load of approximately $\mathcal{O}(cN^2 \log_2 N)$, comparative to the computational load of $\mathcal{O}(c8N^2 \log_2 N)$ for the algorithm that first generates two DTFDs and then correlates them in time and frequency; the constant c is specific to the Fourier transform algorithm used. In addition, we show that the analytic signal could be used in the proposed algorithm, but at a computational cost of four times the computational load of the algorithm using the real-valued signal. Hence we propose using the real-valued signal to minimise the computational load and to avoid a reduction in the performance of the time–frequency matched filter.

2 Background

Here we present some background on the time–frequency matched filter. We review TFDs, the time-domain matched filter, the time–frequency matched filter and finally the discrete time–frequency matched filter.

2.1 Time–frequency distributions

TFDs are used to analyse non-stationary signals because they highlight the time-varying characteristics of these non-stationary signals. Examples of TFD applications include radar and sonar systems [14–16].

There are many different types of TFDs, which can all be grouped into classes. Probably the most commonly used class is the quadratic class of TFDs. At the core of this class is the Wigner–Ville distribution (WVD). The WVD

$$W_s(t,f) = \int_{-\infty}^{\infty} s\left(t+\frac{\tau}{2}\right)s^*\left(t-\frac{\tau}{2}\right)\mathrm{e}^{-\mathrm{j}2\pi\tau f}\,\mathrm{d}\tau$$

is a quadratic function of the time-domain signal $s(t)$. Since the transformation from the time to the time–frequency domain is not linear, the WVD contains cross-terms between the signal's components [17]. Convolving the WVD with the time–frequency kernel $\gamma(t,f)$ can suppress these cross-terms. This smoothed WVD represents the quadratic TFD class $\rho_s(t,f;\,\gamma)$,

$$\rho_s(t,f;\,\gamma) = W_s(t,f) \underset{t}{**}_{f} \gamma(t,f)$$

where different kernels define different distributions in the class.

2.2 Time-domain matched filter

Detecting a known real-valued signal $s(t)$ embedded in a Gaussian noise process $w(t)$ requires a distinction between the two hypotheses H_0 and H_1

$$\begin{aligned} \mathrm{H}_0 &: r(t) = w(t) \\ \mathrm{H}_1 &: r(t) = as(t-t_0)\mathrm{e}^{\mathrm{j}2\pi t f_0} + w(t) \end{aligned} \tag{1}$$

Here, $r(t)$ is the received signal; a is a scaling parameter; $w(t)$ is zero-mean with a constant variance of W_0, that is $\mathrm{E}[w(t)] = 0$ and $\mathrm{var}[w(t)] = W_0$; and the time t_0 and frequency f_0 variables represent time and frequency shifts to the signal $s(t)$.

An example of this detection scenario is the typical radar system. The system transmits a signal $s(t)$ modulated at carrier frequency f_c; thus the transmitted signal is $s(t)\exp(\mathrm{j}2\pi f_\mathrm{c})$. The received signal $r(t)$ may be shifted in time by t_0, the lag value and in frequency by f_0, the Doppler value. Thus

$$r(t) = bs(t-t_0)\mathrm{e}^{\mathrm{j}(2\pi f_\mathrm{c} - 2\pi f_o)(t-t_0)} + w(t)$$

where b is the target reflectivity, $t_0 = 2R/c$, and R is the target's range.

Assuming a small lag-Doppler product of $2\pi f_o t_o \ll 1$, then:

$$r(t) \simeq bs(t-t_0)\mathrm{e}^{\mathrm{j}2\pi f_\mathrm{c}(t-t_0)+\mathrm{j}2\pi f_o t} + w(t)$$

After demodulation, this expression reduces approximately to that in (1) when $a = b\exp(-\mathrm{j}2\pi f_\mathrm{c} t_0)$.

To test the received signal $r(t)$ in (1) for each hypothesis, we compare a test statistic η with a predefined threshold t_h

$$\begin{aligned} \mathrm{H}_0{:}\eta &> t_\mathrm{h} \\ \mathrm{H}_1{:}\eta &< t_\mathrm{h} \end{aligned}$$

When a in (1) is small enough so that the SNR between $s(t)$ and $w(t)$ is small, then the locally optimal test statistic [8] is the bilinear matched filter

$$\eta(t_0,f_0) = \left|\int_{-\infty}^{\infty} r(t)s^*(t-t_0)\mathrm{e}^{-\mathrm{j}2\pi t f_0}\,\mathrm{d}t\right|^2 \tag{2}$$

where we use the generalised likelihood ratio test [8, 9] to obtain the test statistic over the time–frequency area (t_0, f_0),

$$\eta = \max_{(t_0,f_0)} \eta(t_0,f_0)$$

Note that the bilinear matched filter in (2) is equal to the

more familiar ambiguity function

$$\eta(t_0, f_0) = |\chi(-\tau, -\nu)|^2$$

using the notation $t_0 = -\tau$ and $f_0 = -\nu$. The cross-ambiguity function $\chi(\tau, \nu)$ is defined in [6].

2.3 Time–frequency matched filter

We can express the time-domain matched filter in (2) in the time–frequency domain [8, 9] as

$$\eta_{\mathrm{TF}}(t_0, f_0) = \int_{-\infty}^{\infty}\int_{-\infty}^{\infty} W_r(t,f) W_s(t-t_0, f-f_0)\,\mathrm{d}t\,\mathrm{d}f = \left|\int_{-\infty}^{\infty} r(t)s^*(t-t_0)\mathrm{e}^{-\mathrm{j}2\pi t f_0}\,\mathrm{d}t\right|^2 = \eta(t_0, f_0) \tag{3}$$

When $s(t)$ is a random process, we replace the WVD $W_s(t,f)$ in (3) with the Wigner–Ville spectrum (WVS) $\mathrm{E}[W_s(t,f)]$ [17]. For many applications, the WVS is equal to the TFD $\rho_s(t,f;\gamma)$; for example,

- if $s(t)$ is the output of a random time-varying channel with a deterministic input $g(t)$, then $\mathrm{E}[W_s(t,f)] = \rho_g(t,f;S)$, where $S(t,f)$ is the scattering function of the channel [8, 9];
- if $s(t)$ is deterministic, but perturbed in time and frequency by random variables, then $\mathrm{E}[W_s(t,f)] = \rho_s(t,f;G)$, where $G(t,f)$ is the time–frequency probability distribution of the time–frequency perturbation parameters [8]. This is the same as modelling the time t_0 and frequency f_0 shifts as random variables, with $G(t_0, f_0)$ equal to the probability distribution of the shifts, and using the test statistic $\eta_{\mathrm{TF}}(t_0 = 0, f_0 = 0)$ [9];
- if $s(t)$ is not exactly known and is inferred from noisy measurements, then $\mathrm{E}[W_s(t,f)] = \rho_s(t,f;\gamma)$ represents a time–frequency estimate of $s(t)$. The kernel $\gamma(t,f)$ represents the probability distribution of the uncertainty of $s(t)$ [4, 18, 19].

Thus, for many detection scenarios the locally optimum test statistic is

$$\eta_{\mathrm{TF}}(t_0, f_0) = \int_{-\infty}^{\infty}\int_{-\infty}^{\infty} W_r(t,f)\rho_s(t-t_0, f-f_0;\gamma)\,\mathrm{d}t\,\mathrm{d}f \tag{4}$$

This form is a more general expression of the bilinear matched filter: when $\gamma(t,f) = \delta(t)\delta(f)$, then η_{TF} reduces to the bilinear matched filter.

Another advantage of the time–frequency matched filter is that we can time–frequency filter the TFD of $s(t)$, by simply multiplying it with a time–frequency weighting function, known as a mask, $M(t,f)$ [8, 9]. Thus

$$\eta_{\mathrm{TF}}(t_0, f_0) = \int_{-\infty}^{\infty}\int_{-\infty}^{\infty} W_r(t,f)\rho_s(t-t_0, f-f_0;\gamma) \times M(t-t_0, f-f_0)\,\mathrm{d}t\,\mathrm{d}f \tag{5}$$

2.4 Discrete matched filter

Before we can implement the time–frequency matched filter on a computer, we require a discrete version of the filter. We assume that the discrete-time signals $r(nT)$ and $s(nT)$ are Nyquist sampled, where T is the sampling period. When forming the discrete WVD (DWVD) for $r(nT)$ and $s(nT)$, these real-valued signals are usually transformed to discrete analytic signals to avoid aliasing in the DWVD [10–12, 20]. The discrete analytic associate $z_r(nT)$ of the N-point $r(nT)$ is a complex-valued signal of the form

$$z_r(nT) = \begin{cases} r(nT) + \mathrm{j}\mathcal{H}[r(nT)], & 0 \le n \le N-1 \\ 0, & N \le n \le 2N-1 \end{cases}$$

where the function $\mathcal{H}$ represents a discrete version of the Hilbert transform [12]. The analytic signal is zero-padded to length $2N$ to avoid aliasing in the time direction. Fig. 1 shows an example of the DWVD of $r(nT)$ and the DWVD of $z_r(nT)$. Note that the DWVD of the analytic signal $z_r(nT)$ is free from aliasing whereas the DWVD of the real-valued signal is aliased and contains negative–positive frequency cross-terms.

There are different DWVD definitions [10, 11, 20], and care must be taken as some of these definitions do not preserve the mathematical properties of the continuous WVD. For example, the Claasen–Mecklenbräuker DWVD [10] does not satisfy Moyal's formula, an important property for the time–frequency matched filter, whereas the DWVD in [11] does. There is a degradation in performance for the matched filter when the DWVD does not exactly satisfy this property [21, 22].

3 Performance of discrete matched filter

Using the discrete analytic signal introduces error in the time–frequency matched filter. To show this, we form the time–frequency matched filter in (3) at $(t_0 = 0, f_0 = 0)$, using alias-free DWVDs as follows

$$\eta_{\mathrm{TF}}[z_r(nT)] = \sum_{n=0}^{2N-1}\sum_{k=0}^{2N-1} W_{zr}\left(\frac{nT}{2}, \frac{k}{4NT}\right) W_{zs}\left(\frac{nT}{2}, \frac{k}{4NT}\right) = \left|\sum_{n=0}^{N-1} z_r(nT)z_s^*(nT)\right|^2 \tag{6}$$

doi: 10.1049/iet-spr.2009.0104

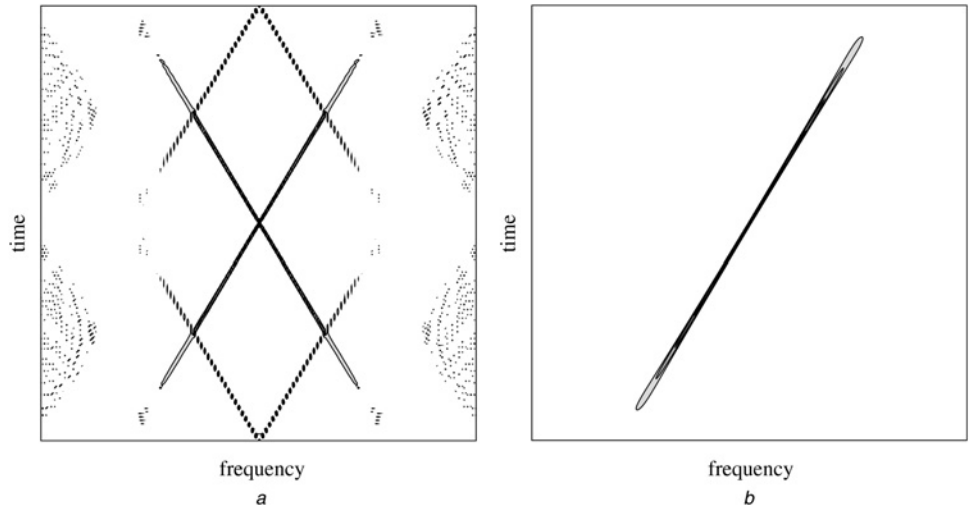

Figure 1 *Aliasing in DWVDs*

a DWVD of real-valued signal
b DWVD of analytic signal
This test signal is a linear frequency modulated signal. The components in *a*, not in *b*, are from by aliasing and negative–positive frequency cross-terms

As $z_s(nT) = s(nT) + \mathrm{j}\mathcal{H}[s(nT)]$ then,

$$\eta_{\mathrm{TF}}[z_r(nT)] = \left| \sum_{n=0}^{2N-1} \{r(nT)s(nT) - \mathcal{H}[r(nT)]\mathcal{H}[s(nT)]\} + \mathrm{j} \sum_{n=0}^{2N-1} \{r(nT)\mathcal{H}[s(nT)] + \mathcal{H}[r(nT)]s(nT)\} \right|^2$$

For the aliased DWVDs, which use the real-valued signals

$$\eta_{\mathrm{TF}}[r(nT)] = \sum_{n=0}^{N-1} \sum_{k=0}^{N-1} W_r\left(\frac{nT}{2}, \frac{k}{2NT}\right) W_s\left(\frac{nT}{2}, \frac{k}{2NT}\right) = \left| \sum_{n=0}^{N-1} r(nT)s^*(nT) \right|^2 \quad (7)$$

which, unlike $\eta_{\mathrm{TF}}[z_r(nT)]$, is equal to a discrete version of the continuous matched filter in (2).

To assess the consequence of the inequality $\eta_{\mathrm{TF}}[z_r(nT)] \neq \eta_{\mathrm{TF}}[r(nT)]$, we use the standard detection performance measure – the deflection criterion for test statistic η [1, 8, 21]

$$d = \frac{|\mathrm{E}(\eta|\mathrm{H}_1) - \mathrm{E}(\eta|\mathrm{H}_0)|}{\{(1/2)[\mathrm{var}(\eta|\mathrm{H}_1) + \mathrm{var}(\eta|\mathrm{H}_0)]\}^{1/2}} \quad (8)$$

For the real-valued signal $r(nT)$, the deflection criterion is [1]

$$d_{\mathrm{RE}} = \sqrt{\frac{E_s}{W_0}} \frac{1}{\sqrt{1 + W_0/E_s}} \quad (9)$$

where E_s is the energy of $s(nT)$ and W_0 is the estimated variance of $w(nT)$, defined as

$$E_s = \frac{1}{N} \sum_{n=0}^{N-1} |s(nT)|^2, \quad W_0 = \frac{1}{N-1} \sum_{n=0}^{N-1} |w(nT)|^2$$

as $w(nT)$ is zero mean. We cannot assume, however, that d_{AN}, the deflection criteria for analytic signal, is similarly defined as d_{RE} is in (9). This is because the discrete analytic signal may not preserve the statistics of the real-valued signal. For example, although $w(nT)$ is zero mean, $z_w(nT)$ may not be zero mean. In addition, the analytic signal $z_s(nT)$ does not preserve the energy of $s(nT)$ [12, 23].

To relate the two performance measures, we define a loss factor Q as:

$$Q = \frac{d_{\mathrm{AN}}}{d_{\mathrm{RE}}} \quad (10)$$

When $Q = 1$, the test statistics $\eta_{\mathrm{TF}}[r(nT)]$ and $\eta_{\mathrm{TF}}[z_r(nT)]$ have the same performance, even though $\eta_{\mathrm{TF}}[z_r(nT)] \neq \eta_{\mathrm{TF}}[r(nT)]$. The inequality $Q < 1$ implies that the matched filter with the real-valued signal better discriminates between the two hypotheses compared to the matched filter with the analytic signal.

We found from experimental estimates of d_{RE} and d_{AN} that Q is approximately always less than one. We used five different signal types for $s(nT)$, and a zero-mean Gaussian random process for $w(nT)$ with a variance of one. Then we computed $\eta_{\mathrm{TF}}[r(nT)]$, using (7), for both hypothesis. To estimate the expectation and variance operators in (8), we used 1000 realisations of $w(nT)$ and thus calculated d_{RE}. Next, we did the same for $\eta_{\mathrm{TF}}[z_r(nT)]$, using (6). For

calculating the discrete analytic signal, we used the method in [12]; we also used the conventional method [10] but found similar results. Note that the energy of the real-valued signal is not equal or proportional to the energy of either of these discrete analytic signals. The five different signal types for $s(nT)$ were an impulse signal, a unit-step signal, a linear frequency modulated signal, a pulse train signal, white Gaussian noise and an underwater recording of a whale cry.

We iterated this whole process over different SNRs and plotted the results in Fig. 2. These findings suggest that the performance is dependent on two things: the signal type and the SNR value. We infer from the results that the matched filter using the real-valued signal is better able to discriminate between the hypotheses than the matched filter with analytic signal.

4 Computation

Here we propose a computational efficient algorithm to implement the time–frequency matched filter, assuming the general form in (4); that is, the matched filter equals the WVD of $r(t)$ correlated with the TFD of $s(t)$. We rewrite (4) as

$$\eta_{\mathrm{TF}}(t_0, f_0) = W_r(t, f) \underset{t}{**}\underset{f}{} \rho_s(-t, -f; \gamma)$$

using the correlation–convolution relation $a(t) \bigstar b(t) = a(t) * b(-t)$, where $\bigstar$ represents the correlation and $*$ represents convolution, and $a(t)$, $b(t)$ are arbitrary real-valued functions.

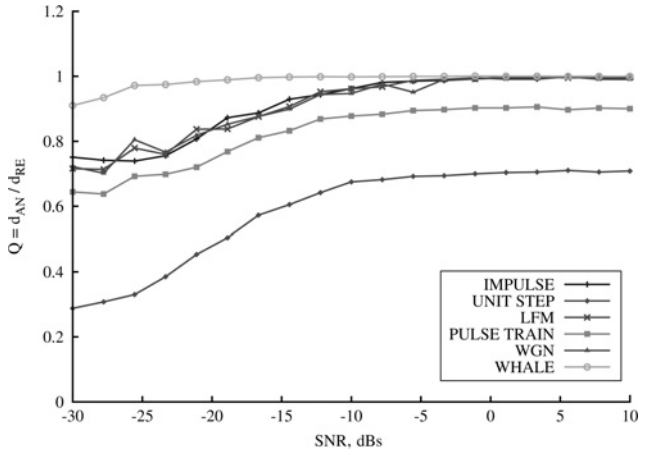

Figure 2 *Loss factor Q for different signals over different SNR values*

A value of $Q < 1$ implies that the matched filter using the real-valued signal outperforms the matched filter using the analytic signal. The six different signal types are an impulse signal, a unit-step signal, a linear frequency modulated signal (LFM) signal, a white Gaussian noise (WGN) signal and an underwater recording of a whale cry

Separating the kernel from the WVDs

$$\eta_{\mathrm{TF}}(t_0, f_0) = [W_r(t, f) \underset{t}{**}\underset{f}{} W_s(-t, -f)] \underset{t}{**}\underset{f}{} \gamma(t, f)$$

$$= \left| \int_{-\infty}^{\infty} r(t) s^*(t - t_0) \mathrm{e}^{-\mathrm{j}2\pi t f_0} \, \mathrm{d}t \right|^2 \underset{t}{**}\underset{f}{} \gamma(t, f)$$

In discrete form, for N-point real-valued signals $r(nT)$ and $s(nT)$,

$$\eta_{\mathrm{TF}}\left(nT, \frac{k}{NT}\right) = \left| \sum_{m=0}^{N-1} r(mT) s((m-n)T) \mathrm{e}^{-\mathrm{j}2\pi mk/N} \right|^2 \underset{n}{\circledast}\underset{k}{\circledast} \gamma\left(n, \frac{k}{NT}\right) \tag{11}$$

where $\circledast$ represents the circular convolution operation. We shall use the notation

$$\left| F_s^r\left(nT, \frac{k}{NT}\right) \right|^2 = \left| \sum_{m=0}^{N-1} r(mT) s((m-n)T) \mathrm{e}^{-\mathrm{j}2\pi mk/N} \right|^2$$

where $|F_s^r(nT, k/NT)|^2$ is the spectrogram of signal $s(nT)$ with window $r(nT)$ [9].

4.1 Algorithm

The following algorithm implements (11) with a minimal computational load. We implement the convolution operation in (11) by multiplying two functions in the Doppler–lag domain. Thus, we require to discrete Fourier transform (DFT) the spectrogram $|F_s^r(nT, k/NT)|^2$ to the Doppler–lag domain. Rather than first forming the spectrogram and then mapping to the Doppler–lag domain, which requires the following processes

$$\text{time–lag} \xrightarrow{\text{DFT}} \text{time–frequency} \xrightarrow{\text{IDFT}}$$
$$\text{time–lag} \xrightarrow{\text{DFT}} \text{Doppler–lag}$$

we skip the first DFT and inverse DFT (IDFT) operations and reduce the processes to:

$$\text{time–lag} \xrightarrow{\text{DFT}} \text{Doppler–lag.} \tag{12}$$

We do this by using the relation

$$\underset{k \to m}{\text{IDFT}} \left\{ \underset{n \to l}{\text{DFT}} \left\{ \left| F_s^r\left(nT, \frac{k}{NT}\right) \right|^2 \right\} \right\} = A_r\left(\frac{l}{NT}, mT\right) A_s^*\left(\frac{l}{NT}, mT\right) \tag{13}$$

where $A_r(l/NT, mT)$ and $A_s(l/NT, mT)$ are discrete ambiguity functions (AFs); the proof for this relation is in the Appendix. Also, the algorithm takes advantage of the

doi: 10.1049/iet-spr.2009.0104

conjugate symmetric relation:

$$A_r\left(\frac{l}{NT}, -mT\right)A_s^*\left(\frac{l}{NT}, -mT\right) = A_r^*\left(\frac{l}{NT}, mT\right)A_s\left(\frac{l}{NT}, mT\right)$$

This relation is a consequence of (13): as the spectrogram is a real-valued function, the DFT of the spectrogram must be conjugate symmetrical [24].

The complete algorithm is as follows. (We assume that Doppler–lag kernel is conjugate symmetrical in the lag direction; this condition ensures that the test statistic is real valued.)

• INPUT: N-point real-valued received signal $r(nT)$; $N \times (N_h + 1)$ Doppler–lag kernel $g(l/NT, mT)$.

• OUTPUT: $N \times N$ time–frequency test statistic $\eta_{TF}(nT, k/NT)$.

1. Form the time–lag functions $K_r(nT, mT)$ and $K_s(nT, mT)$:

$$K_r(nT, mT) = r(nT)r((n-m)T)$$
$$K_s(nT, mT) = s(nT)s((n-m)T)$$

for $0 \le n \le N-1$ and $0 \le m \le N_h$, where $N_h = \lceil N/2 \rceil$.

2. DFT both $N \times (N_h + 1)$ time–lag functions to the Doppler–lag domain:

$$A_r\left(\frac{l}{NT}, mT\right) = \underset{n \to l}{\text{DFT}}\{K_r(nT, mT)\}$$
$$A_s\left(\frac{l}{NT}, mT\right) = \underset{n \to l}{\text{DFT}}\{K_s(nT, mT)\}$$

for $0 \le m \le N_h$. Note in the Appendix how we define these discrete AFs.

3. Multiply these two discrete AFs with the kernel as follows

$$S\left(\frac{l}{NT}, mT\right) = A_r\left(\frac{l}{NT}, mT\right) \times A_s^*\left(\frac{l}{NT}, mT\right)g\left(\frac{l}{NT}, mT\right)$$

over $0 \le n \le N-1$ and $0 \le m \le N_h$.

4. IDFT back to the time–lag domain,

$$R(nT, mT) = \underset{l \to n}{\text{IDFT}}\left\{S\left(\frac{l}{NT}, mT\right)\right\}$$

for $0 \le m \le N_h$.

5. Recover the negative lag values from the positive ones:

$$R(nT, (N-m)T) = R(nT, mT), \quad 1 \le m \le N_h - 1$$

for $0 \le n \le N-1$.

6. DFT to the time–frequency domain

$$\eta_{TF}\left(nT, \frac{k}{NT}\right) = \underset{m \to k}{\text{DFT}}\{R(nT, mT)\}$$

for $0 \le n \le N-1$.

4.2 Computational complexity

The majority of the computational complexity for the matched filter is from the number of DFTs in the algorithm. Thus, we count the DFTs in the algorithm to assess the computational load. When quantifying this load, we assume that the Doppler–lag kernel $g(l/NT, mT)$ is real valued, which is true for almost all TFDs [17].

Using the notation $1 \times$ RDFT-N to represent one real-valued N-point DFT operation, we quantify the computational load as follows. The discrete AFs A_s and A_r require $2N_h \times$ RDFT-N operations and the time–lag function R requires $N_h \times$ inverse RDFT-N operations. To DFT R from the time–lag to the time–frequency domain, we use a real-symmetric DFT algorithm [25], which requires the equivalent load of $N/2 \times$ RDFT-N operations. Thus, the algorithm requires a total load of approximately $2N \times$ RDFT-N operations.

Fast Fourier transform algorithms can implement RDFT-N and inverse RDFT-N operations with $\mathcal{O}(cN/2 \log_2 N)$ multiplications and additions, where c is a constant that depends on the specific algorithm [26, 27]. Hence the time–frequency matched filter algorithm requires a total computational load of $\mathcal{O}(cN^2 \log_2 N)$. If we were to use the discrete analytic signal in this algorithm then the load would increase to $\mathcal{O}(c4N^2 \log_2 2N)$, more than four times the load of the algorithm with the real-valued signals.

The direct approach is to implement the matched filter as a discrete version of (4). This method forms the alias-free DWVD and DTFD and then correlates, in time and frequency, these two functions [5, 18, 19]. It is important to use a DWVD and DTFD that satisfies Moyal's formula, otherwise the performance of the detector degrades [21, 22]. We thus use the DTFD proposed in [13], which satisfies Moyal's formula. The DTFD and DWVD require a total load of $\mathcal{O}(4N^2 \log_2 N)$ [11, 28], and to convolve these function in time–frequency requires an extra load of approximately $\mathcal{O}(4N^2 \log_2 N)$. Hence the total load for this method is $\mathcal{O}(8N^2 \log_2 N)$.

Sayeed in [9] proposes using the sum-of-spectrograms method [29] to approximate the matched filter. This

method decomposes the kernel into eigenvalues and eigenvectors and then approximates the DTFD by summing only a smaller number of eigenvalues weighted by the spectrograms of the signal and eigenvectors. The method requires a computational load of $\mathcal{O}(cLN^2/4\log_2 N)$, where $1 \le L \le 2N-1$ is the number of eigenvalues used in the approximation. Table 1 summarises the computational load for the various methods.

When the received signal $r(nT)$ is of infinite or long duration, the common practice is to use a sliding window on $r(nT)$ and process each windowed segment separately. Thus, $s(nT)$ remains the same but $r(nT)$ changes over repeated matched-filtering operations. We can therefore pre-compute $A_s(l/NT, mT)$ and use this array as an input to the proposed algorithm and save the computational load of having to repetitively compute $A_s(l/NT, mT)$. The computational load for this algorithm is $\mathcal{O}(c3N^2/4\log_2 N)$, which reduces the computational load of the proposed algorithm by one-quarter.

4.3 Algorithm incorporating time–frequency filtering

Here we augment the matched filter algorithm to incorporate time–frequency filtering. This algorithm implements a discrete version of (5). First to do the filtering, we compute the DWVD of $s(nT)$, then filter the DWVD in the time–frequency domain, and then DFT to the Doppler–lag domain to obtain the resultant discrete AF. Next, we use this discrete AF in the matched filter algorithm.

The first part of the algorithm, using the time–frequency filter $M(nT, k/NT)$, generates the time–frequency filtered AF as follows:

1. Form the time–lag function,

$$K_s(nT, m2T) = s((n+m)T)s((n-m)T)$$

$$K_s\left(\left(n+\frac{1}{2}\right)T, m2T\right) = s((n+m+1)T)s((n-m)T)$$

for $0 \le n \le N-1$ and $0 \le m \le N_h$ and recover the negative lag values from the positives ones [28]

$$K_s(nT, (N-m)2T) = K_s(nT, m2T)$$

for $1 \le m \le N_h - 1$ and

$$K_s\left(\left(n+\frac{1}{2}\right)T, (N-m-1)2T\right) = K_s\left(\left(n+\frac{1}{2}\right)T, m2T\right)$$

for $0 \le m \le N_h - 1$.

2. DFT to the time–frequency domain

$$W_s\left(\frac{nT}{2}, \frac{k}{2NT}\right) = \underset{m\to k}{\mathrm{DFT}}\left\{K^s\left(\frac{nT}{2}, m2T\right)\right\}$$

for $0 \le n \le N-1$. We do not modulate this DWVD with the required complex exponential [20] because, in the following steps, we transform the (masked) WVD back to the time–lag domain and the multiplication and division of the exponential cancel [28].

3. Time–frequency filter, let

$$W_s^M\left(\frac{nT}{2}, \frac{k}{2NT}\right) = W_s\left(\frac{nT}{2}, \frac{k}{2NT}\right)M\left(\frac{nT}{2}, \frac{k}{2NT}\right)$$

4. Then, DFT back to the time–lag domain

$$K_s^M\left(\frac{nT}{2}, mT\right) = \underset{k\to m}{\mathrm{IDFT}}\left\{W_s^M\left(\frac{nT}{2}, mT\right)\right\}$$

5. Reorder the array as follows

$$R_s^{\mathrm{d}}(nT, m2T) = R_s^M(nT, m2T)$$

$$R_s^{\mathrm{d}}\left(nT, \left(m+\frac{1}{2}\right)2T\right) = R_s^M\left(\left(n+\frac{1}{2}\right)T, m2T\right)$$

over $0 \le N \le N-1$ and $0 \le m \le N$. Note that this is a simple reordering of the position of the elements in the array R_s^M [28].

6. DFT to the Doppler–lag domain

$$A_s^M\left(\frac{l}{NT}, mT\right) = \underset{n\to l}{\mathrm{DFT}}\{R_s^{\mathrm{d}}(nT, mT)\}$$

for $0 \le m \le N_h$.

The complete algorithm, using the time–frequency filtered AF A_s^M, implements the matched filter as follows:

• INPUT: N-point real-valued received signal $r(nT)$; $N \times (N_h+1)$ Doppler–lag kernel $g(l/NT, mT)$; and $N \times (N_h+1)$ AF $A_s^M(l/NT, mT)$.

Table 1 Computational complexity to compute the matched filter on an N-point signal

Method	Signal type	Computational load
Proposed algorithm	real	$\mathcal{O}(cN^2 \log_2 N)$
Proposed algorithm	analytic	$\mathcal{O}(c4N^2 \log_2 2N)$
DTFD	analytic	$\mathcal{O}(c8N^2 \log_2 N)$
Sum-of-spectrogram	real	$\mathcal{O}(cLN^2/4 \log_2 N)$

The sum-of-spectrogram method approximates the matched filter for $L < 2N$

IET Signal Process., 2010, Vol. 4, Iss. 4, pp. 428–437
doi: 10.1049/iet-spr.2009.0104

• OUTPUT: $N \times N$ time–frequency test statistic $\eta_{\mathrm{TF}}(nT, k/NT)$.

1. Form the time–lag function K_r

$$K_r(nT, m2T) = s((n+m)T)s((n-m)T)$$

$$K_r\left(nT, \left(m+\frac{1}{2}\right)2T\right) = s((n+m+1)T)s((n-m)T)$$

for $0 \le n \le N-1$ and $0 \le m \le N_{\mathrm{h}}$.

2. DFT $N \times (N_{\mathrm{h}}+1)$ K_r to the Doppler–lag domain

$$A_r\left(\frac{l}{NT}, mT\right) = \underset{n \to l}{\mathrm{DFT}}\{K_r(nT, mT)\}$$

for $0 \le m \le N_{\mathrm{h}}$.

3. Multiply the two ambiguity functions with the kernel

$$S\left(\frac{l}{NT}, mT\right) = A_r\left(\frac{l}{NT}, mT\right) \times \left[A_s^M\left(\frac{l}{NT}, mT\right)\right]^* g\left(\frac{l}{NT}, mT\right)$$

over $0 \le n \le N-1$ and $0 \le m \le N_{\mathrm{h}}$.

4. To complete, follow steps 4–6 of the algorithm in Section 4.1.

This algorithm requires the same computational load as that for the matched filter in Section 4.1 assuming that we pre-compute $A_s(l/NT, mT)$; this load is $\mathcal{O}(c3N^2/4\log_2 N)$.

5 Conclusions

The discrete time–frequency matched filter correlates two discrete TFDs. When we use aliased discrete TFDs, the discrete matched filter is a discrete version of the continuous matched filter. When we use alias-free discrete TFDs – and therefore the analytic, rather than real valued, signal – the discrete matched filter does not equal a discrete version of the continuous matched filter. This is because the test statistic contains extra terms involving the products of real and imaginary parts of the analytic signal. We have yet to determine the precise effects of these extras terms on the performance of the detector. What we can infer from the simulation results, however, is that using the analytic signal degrades the performance of the matched filter. The results also showed that this relative performance was dependent on the SNR and the type of signal. Theoretical analysis may shed some insight into why this relative performance varies with SNR and signal characteristics. Nonetheless, because of this unknown quantity of performance degradation – and because the algorithm with the real-valued signal requires only one-quarter of the computational load of the algorithm with the analytic signal – we recommend using the real-valued signal in the time–frequency matched filter. Matlab and Octave code to accompany this article is available to download at http://espace.library.uq.edu.au/view/UQ:185230.

6 References

[1] BOASHASH B., O' SHEA P.: 'A methodology for detection and classification of some underwater acoustic signals using time–frequency analysis techniques', *IEEE Trans. Acoust., Speech, Signal Process.*, 1990, **38**, (11), pp. 1829–1841

[2] CHEN V.C.: 'Radar ambiguity function, time-varying matched filter, and optimum wavelet correlator', *Opt. Eng.*, 1994, **2242**, pp. 337–345

[3] WEN C., DOHERTY J., MATHEWS J.: 'Time–frequency radar processing for meteor detection', *IEEE Trans. Geosci. Remote Sens.*, 2004, **42**, (3), pp. 501–510

[4] RICHARD C., LENGELLE R.: 'Joint time and time–frequency optimal detection of K-complexes in sleep EEG', *Comput. Biomed. Res.*, 1998, **31**, (3), pp. 209–229

[5] O' TOOLE J.M., MESBAH M., BOASHASH B., COLDITZ P.: 'A new neonatal seizure detection technique based on the time–frequency characteristics of the electroencephalogram'. Proc. Int. Sym. on Signal Processing and its Applications, ISSPA-07, Sharjah, United Arab Emirates, 12–15 February 2007, vol. III, pp. 132–135

[6] SINSKY A., WANG C.: 'Standardization of the definition of the radar ambiguity function', *IEEE Trans. Aerosp. Electron. Syst.*, 1974, **10**, (4), pp. 532–533

[7] KAILATH T., POOR H.: 'Detection of stochastic processes', *IEEE Trans. Inf. Theory*, 1998, **44**, (6), pp. 2230–2259

[8] FLANDRIN P.: 'A time–frequency formulation of optimum detection', *IEEE Trans. Acoust., Speech, Signal Process.*, 1988, **36**, (9), pp. 1377–1384

[9] SAYEED A.: 'Optimal time–frequency detectors', in BOASHASH B. (ED.): 'Time–frequency signal analysis and processing: a comprehensive reference' (Elsevier, Oxford, UK, 2003), Ch. 12, pp. 500–509

[10] CLAASEN T., MECKLENBRÄUKER W.: 'The Wigner distribution–a tool for time–frequency signal analysis. Part II: discrete-time signals', *Philips J. Res.*, 1980, **35**, pp. 276–350

[11] O' TOOLE J., MESBAH M., BOASHASH B.: 'A discrete time and frequency Wigner–Ville distribution: properties and implementation'. Proc. Int. Conf. on Digital Signal Processing and Comm. Systems, Noosa Heads, Australia, 19–21 December 2005, vol. CD-ROM, [Online], available at: http://eprints.qut.edu.au/2607/

[12] O' TOOLE J.M., MESBAH M., BOASHASH B.: 'A new discrete analytic signal for reducing aliasing in the discrete Wigner–Ville distribution', *IEEE Trans. Signal Process.*, 2008, **56**, (11), pp. 5427–5434

[13] O' TOOLE J.M., MESBAH M., BOASHASH B.: 'Improved discrete definition of quadratic time–frequency distributions', *IEEE Trans. Signal Process.*, 2010, **58**, (2), pp. 906–911

[14] CHEN V.: 'Doppler signatures of radar backscattering from objects with micro-motions', *IET Signal Process.*, 2008, **2**, (3), pp. 291–300

[15] THAYAPARAN T., KENNEDY S.: 'Detection of a manoeuvring air target in sea-clutter using joint time–frequency analysis techniques', *IEE Proc. Radar, Sonar Navig.*, 2004, **151**, (1), pp. 19–30

[16] ZHANG Y., QIAN S., THAYAPARAN T.: 'Detection of a manoeuvring air target in strong sea clutter via joint time–frequency representation', *IET Signal Process.*, 2008, **2**, (3), pp. 216–222

[17] BOASHASH B.: 'Part I: introduction to the concepts of TFSAP', in BOASHASH B. (ED.): 'Time–frequency signal analysis and processing: a comprehensive reference' (Elsevier, Oxford, UK, 2003), Ch. 1–3, pp. 3–76

[18] MELLINGER D.K., CLARK C.W.: 'Recognizing transient low-frequency whale sounds by spectrogram correlation', *J. Acoust. Soc. Am.*, 2000, **107**, (6), pp. 3518–3529

[19] BOASHASH B., MESBAH M.: 'Time–frequency methodology for newborn electroencephalographic seizure detection', in PAPANDREOU-SUPPAPPOLA A. (ED.): 'Applications in time–frequency signal processing' (CRC Press, 2003), Ch. 9, pp. 339–369

[20] PEYRIN F., PROST R.: 'A unified definition for the discrete-time, discrete-frequency, and discrete-time/frequency Wigner distributions', *IEEE Trans. Acoust., Speech, Signal Process.*, 1986, **34**, (4), pp. 858–866

[21] KUMAR B.V., CARROLL C.: 'Effects of sampling on signal detection using the cross-Wigner distribution function', *Appl. Opt*, 1984, **23**, pp. 4090–4094

[22] RICHARD C.: 'Time–frequency based detection using discrete-time discrete-frequency Wigner distributions', *IEEE Trans. Signal Process.*, 2002, **50**, (9), pp. 2170–2176

[23] MARPLE S.L. JR.: 'Computing the discrete-time 'analytic' signal via FFT', *IEEE Trans. Signal Process.*, 1999, **47**, (9), pp. 2600–2603

[24] OPPENHEIM A.V., SCHAFER R.W.: 'Discrete-time signal processing' (Prentice-Hall, Englewood Cliffs, NJ, 1999)

[25] DUHAMEL P.: 'Implementation of "split-radix" FFT algorithms for complex, real and real-symmetric data', *IEEE Trans. Acoust., Speech, Signal Process*, **34**, (2), pp. 285–295

[26] DUHAMEL P., VETTERLI M.: 'Fast fourier transforms: a tutorial review and a state of the art', *Signal Process.*, 1990, **19**, pp. 259–299

[27] FRIGO M., JOHNSON S.G.: 'The design and implementation of FFTW3', *Proc. IEEE*, 2005, **93**, (2), pp. 216–231; special issue on 'Program generation, optimization, and platform adaptation'

[28] O' TOOLE J.M., MESBAH M., BOASHASH B.: 'Algorithms for discrete quadratic time–frequency distributions', *WSEAS Trans. Signal Process.*, invited paper', 2008, **4**, (5), pp. 320–329

[29] CUNNINGHAM G., WILLIAMS W.: 'Fast implementations of generalized discrete time–frequency distributions', *IEEE Trans. Signal Process.*, 1994, **42**, (6), pp. 1496–1508

7 Appendix: proof of spectrogram–ambiguity function relation

Here we prove the relation in (13). This relation relates the spectrogram to discrete AFs. For this proof, we rewrite (13) as

$$\left|F_s^r\left(nT, \frac{k}{NT}\right)\right|^2 = \underset{m\to k}{\mathrm{DFT}}\left\{\underset{l\to n}{\mathrm{IDFT}}\left\{A_r\left(\frac{l}{NT}, mT\right) \times A_s^*\left(\frac{l}{NT}, mT\right)\right\}\right\} \tag{14}$$

where $|F_s^r|^2$ represents the spectrogram

$$\left|F_s^r\left(nT, \frac{k}{NT}\right)\right|^2 = \left|\sum_{m=0}^{N-1} r(mT)s((m-n)T)\mathrm{e}^{-\mathrm{j}2\pi mk/N}\right|^2$$

We define the AF A_r as

$$A_r\left(\frac{l}{NT}, mT\right) = \sum_{n=0}^{N-1} r(nT)r((n-m)T)\mathrm{e}^{-\mathrm{j}2\pi nl/N}$$

(We omit the modulation term, usually used with the anti-symmetric time–lag function $r(nT)r((n-m)T)$ [20], as it cancels on the forward and inverse DFT operations.)

doi: 10.1049/iet-spr.2009.0104

To start, we expand the spectrogram as follows

$$\begin{aligned}\left|F_s^r\left(nT,\frac{k}{NT}\right)\right|^2 &= F_s^r\left(nT,\frac{k}{NT}\right)\left[F_s^r\left(nT,\frac{k}{NT}\right)\right]^* \\ &= \underset{m\to k}{\mathrm{DFT}}\Big\{[x(mT)y((m-n)T)] \\ &\quad \circledast_m [x(-mT)y((-m-n)T)]\Big\} \\ &= \sum_{p=0}^{N-1} x(pT)y((p-n)T) \\ &\quad \times \sum_{m=0}^{N-1} x((p+m)T)y((p+m-n)T)\mathrm{e}^{-\mathrm{j}2\pi mk/N}\end{aligned} \tag{15}$$

where $\circledast$ represents the circular convolution.

In the Doppler–lag domain we have

$$\begin{aligned}&A_r\left(\frac{l}{NT}, mT\right)A_s^*\left(\frac{l}{NT}, mT\right) \\ &= \sum_{n_1=0}^{N-1}\sum_{n_2=0}^{N-1} x(n_1T)x((n_1-m)T) \\ &\quad \times y(n_2T)y((n_2-m)T)\mathrm{e}^{-\mathrm{j}2\pi(n_1-n_2)l/N}\end{aligned}$$

We map these AF products to the time–lag domain

$$\underset{l\to m}{\mathrm{IDFT}}\left\{A_r\left(\frac{l}{NT}, mT\right)A_s^*\left(\frac{l}{NT}, mT\right)\right\}$$

$$\begin{aligned}&= \sum_{n_1=0}^{N-1}\sum_{n_2=0}^{N-1} x(n_1T)x((n_1-m)T)y(n_2T)y((n_2-m)T) \\ &\quad \times \sum_{l=0}^{N-1}\mathrm{e}^{-\mathrm{j}2\pi(n_1-n_2-n)l/N}\end{aligned}$$

The sum of the exponential term in this expression equates to the Dirac function $\delta(n_1-n_2-n)$ and therefore this expression reduces to

$$\sum_{n_2=0}^{N-1} y(n_2T)y((n_2-m)T)x((n_2+n)T)x((n_2+n-m)T)$$

Mapping this time–lag function to the time-frequency domain, we obtain

$$\begin{aligned}&\underset{m\to k}{\mathrm{DFT}}\left\{\underset{l\to m}{\mathrm{IDFT}}\left\{A_r\left(\frac{l}{NT}, mT\right)A_s^*\left(\frac{l}{NT}, mT\right)\right\}\right\} \\ &= \sum_{m=0}^{N-1}\sum_{n_2=0}^{N-1} y(n_2T)y((n_2-m)T)x((n_2+n)T) \\ &\quad \times x((n_2+n-m)T)\mathrm{e}^{-\mathrm{j}2\pi mk/N}\end{aligned}$$

By letting $q = p-n+m$

$$\begin{aligned}&\underset{m\to k}{\mathrm{DFT}}\left\{\underset{l\to m}{\mathrm{IDFT}}\left\{A_r\left(\frac{l}{NT}, mT\right)A_s^*\left(\frac{l}{NT}, mT\right)\right\}\right\} \\ &= \sum_{q=0}^{N-1} x(qT)y((q-n)T) \\ &\quad \times \sum_{m=0}^{N-1} x((q+m)T)y((q+m-n)T)\mathrm{e}^{-\mathrm{j}2\pi mk/N}\end{aligned}$$

which is equal to (15) thus proving the relation in (14).

doi: 10.1049/iet-spr.2009.0104